

3D Printing/Interfacial Polymerization Coupling for the Fabrication of Conductive Hydrogel

*Original*

3D Printing/Interfacial Polymerization Coupling for the Fabrication of Conductive Hydrogel / Fantino, E., Roppolo, I., Zhang, D., Xiao, J., Chiappone, A., Castellino, M., Guo, Q., Pirri, C.F., Yang, J.. - In: MACROMOLECULAR MATERIALS AND ENGINEERING. - ISSN 1438-7492. - 303:4(2018), p. 1700356. [10.1002/mame.201700356]

*Availability:*

This version is available at: 11583/2732601 since: 2020-03-31T15:05:35Z

*Publisher:*

Wiley-VCH Verlag

*Published*

DOI:10.1002/mame.201700356

*Terms of use:*

This article is made available under terms and conditions as specified in the corresponding bibliographic description in the repository

*Publisher copyright*

(Article begins on next page)



Postfach 10 11 61  
69451 Weinheim  
Germany

*Courier services:*  
Boschstraße 12  
69469 Weinheim  
Germany

Tel.: (+49) 6201 606 581

Fax: (+49) 6201 606 510

E-mail: [macromol@wiley-vch.de](mailto:macromol@wiley-vch.de)

WILEY-VCH

---

Dear Author,

**Please correct your galley proofs carefully and return them no more than four days after the page proofs have been received.**

The editors reserve the right to publish your article without your corrections if the proofs do not arrive in time.

Note that the author is liable for damages arising from incorrect statements, including misprints.

Please note any queries that require your attention. These are indicated with a Q in the PDF and a question at the end of the document.

**Please limit corrections to errors already in the text; cost incurred for any further changes or additions will be charged to the author, unless such changes have been agreed upon by the editor.**

**Reprints** may be ordered by filling out the accompanying form.

Return the reprint order form by fax or by e-mail with the corrected proofs, to Wiley-VCH : [macromol@wiley-vch.de](mailto:macromol@wiley-vch.de)

To avoid commonly occurring errors, please ensure that the following important items are correct in your proofs (please note that once your article is published online, no further corrections can be made):

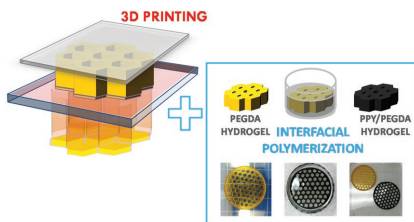
- **Names** of all authors present and spelled correctly
- **Titles** of authors correct (Prof. or Dr. only: please note, Prof. Dr. is not used in the journals)
- **Addresses** and **postcodes** correct
- **E-mail address** of corresponding author correct (current email address)
- **Funding bodies** included and grant numbers accurate
- **Title** of article OK
- All **figures** included
- **Equations** correct (symbols and sub/superscripts)

**Corrections should be made directly in the PDF file using the PDF annotation tools. If you have questions about this, please contact the editorial office. The corrected PDF and any accompanying files should be uploaded to the journal's Editorial Manager site.**

xxxx

E. Fantino,\* I. Roppolo, D. Zhang,  
J. Xiao, A. Chiappone, M. Castellino,  
Q. Guo, C. F. Pirri, J. Yang\* ..... 1700356

**3D Printing/Interfacial Polymerization  
Coupling for the Fabrication of  
Conductive Hydrogel**



**3D printing** is coupled with interfacial polymerization to obtain electroactive hydrogels with complex and defined geometry. Conductive hydrogels are created through a two-step procedure: first a digital light processing 3D printing system is used to fabricate 3D structures and then pyrrole is oxidized to polypyrrole, exploiting an interfacial polymerization mechanism, thus creating a conductive phase directly in 3D printed structure.

Q1

1  
2  
3  
4  
5  
6  
7  
8  
9  
10  
11  
12  
13  
14  
15  
16  
17  
18  
19  
20  
21  
22  
23  
24  
25  
26  
27  
28  
29  
30  
31  
32  
33  
34  
35  
36  
37  
38  
39  
40  
41  
42  
43  
44  
45  
46  
47  
48  
49  
50  
51  
52  
53  
54  
55  
56  
57  
58  
59

1  
2  
3  
4  
5  
6  
7  
8  
9  
10  
11  
12  
13  
14  
15  
16  
17  
18  
19  
20  
21  
22  
23  
24  
25  
26  
27  
28  
29  
30  
31  
32  
33  
34  
35  
36  
37  
38  
39  
40  
41  
42  
43  
44  
45  
46  
47  
48  
49  
50  
51  
52  
53  
54  
55  
56  
57  
58  
59

UNCORRECTED PROOF



# 3D Printing/Interfacial Polymerization Coupling for the Fabrication of Conductive Hydrogel

Erika Fantino,\* Ignazio Roppolo, Dongxing Zhang, Junfeng Xiao, Annalisa Chiappone, Micaela Castellino, Qiuquan Guo, Candido Fabrizio Pirri, and Jun Yang\*

In this study, 3D printing is coupled with interfacial polymerization to obtain electroactive hydrogels with complex and defined geometry. Conductive hydrogels are created through a two-step procedure: first a digital light processing 3D printing system is used to fabricate poly(ethylene glycol)diacrylate 3D structure and then pyrrole is oxidized to polypyrrole (PPY), exploiting an interfacial polymerization mechanism thanks to which PPY can be formed into the poly(ethylene glycol) matrix, thus creating a conductive phase.

## 1. Introduction

Recently, conductive hydrogels have attracted much interest in the field of biomaterials science being able to combine highly hydrated polymer structures with intriguing electronic functionalities.<sup>[1,2]</sup> These hybrid materials, merging the hydrogel characteristics with the advantages of the conductive components such as electrical conductivity and electrochemical-redox properties, have found applications across a range of biomedical applications such as biosensors, drug delivery, and tissue engineering.<sup>[3,4]</sup> In these composite hydrogels, conductivity was achieved either incorporating electrically conductive fillers, such as graphite, metallic particles, and carbon nanotubes,<sup>[5–7]</sup> or integrating intrinsically conductive polymers within the hydrogel matrix.

Conductive polymers are macromolecules with conjugated backbone; examples are polyacetylene, polythiophene, polypyrrole (PPY), or polyaniline. In recent years they have received great interest owing to their ability to conduct electricity and they have been used in several biomedical applications.<sup>[4,8–11]</sup>

E. Fantino, Prof. C. F. Pirri  
Department of Applied Science and Technology  
Politecnico di Torino  
Corso Duca degli Abruzzi 24, Torino 10129, Italy  
E-mail: erika.fantino@polito.it

I. Roppolo, A. Chiappone, M. Castellino, Prof. C. F. Pirri  
Center for Sustainable Futures@Polito  
Istituto Italiano di Tecnologia  
Corso Trento 21, Torino 10129, Italy

D. Zhang, J. Xiao, Q. Guo, Prof. J. Yang  
Department of Mechanical and Materials Engineering  
The University of Western Ontario  
London, Ontario, N6A 5B9, Canada  
E-mail: jyang@eng.uwo.ca

The ORCID identification number(s) for the author(s) of this article can be found under <https://doi.org/10.1002/mame.201700356>.

DOI: 10.1002/mame.201700356

Conductive hydrogels exploiting intrinsically conducting polymers allow obtaining materials that further expand the application area of hydrogels<sup>[12–14]</sup> driving researchers to develop new fabrication methods.

The fabrication of conductive hydrogels with particular geometry and controlled features is still a big issue. 3D printing is an additive manufacturing (AM) process that enables to construct 3D objects directly from a digital model. It has

received a great deal of attention from a diverse range of fields including electronics,<sup>[14]</sup> biomedics and regenerative medicine,<sup>[15–17]</sup> and microfluidics.<sup>[18]</sup> Objects are constructed layer-by-layer, enabling the creation of complex parts with tailored morphology and functionality.<sup>[19]</sup> There exist several different 3D printing techniques that differ from each other for the kind of polymer that is used (i.e., thermoplastic or thermosetting) and for the technology beyond the building process.<sup>[16]</sup> One of the most widely used 3D printing processes, namely, vat polymerization, is based on photopolymerization. Stereolithography (SLA), a well-established AM technology, is used to create thermoset objects with features <100 μm by selectively scanning an ultraviolet (UV) laser beam across a reservoir of photopolymer resin.<sup>[19]</sup> Another 3D printing process based on spatially controlled solidification of a liquid resin by photopolymerization is digital light processing (DLP). Instead of using a laser to “draw” the object under a point-by-point manner like in SLA, DLP equipment projects an entire slice of an object using a digital projector.<sup>[20]</sup> Both techniques provide powerful tools to fabricate complex 3D polymeric structures, with good resolution and fast production times especially in the case of DLP. This opens infinite possibilities in their design and applications.<sup>[21–25]</sup>

Many types of hydrogels have been reported in the literature including natural materials or synthetic ones.<sup>[16,26,27]</sup> Among the synthetic polymers, poly(ethylene glycol) (PEG) based ones have been used extensively for the fabrication of hydrogels thanks to their well-known hydrophilicity and biocompatibility.<sup>[28,29]</sup> With acrylated or methacrylated moieties, PEG monomers can be photocrosslinked in the presence of appropriate initiating agents and the use of SLA or DLP has also been reported as a successful method for fabricating complex functional 3D structures based on PEG monomer materials.<sup>[23,30–33]</sup> The choice of relatively low molecular weight ( $M_w$  500–700) PEG-based acrylate monomers allows preparing reactive formulations with sufficiently low viscosity to be processed with a fast and low-cost DLP apparatus giving self-standing and robust

1 structures thanks to the crosslink density reached in this  
2 kind of network.<sup>[34]</sup> Herein, the strategy we developed within  
3 this study consists in coupling interfacial polymerization<sup>[8,35–37]</sup>  
4 with 3D printing in order to obtain electroactive hydrogel  
5 with complex and defined geometry. After 3D printing of the  
6 hydrogel structures, a chemical oxidative polymerization of pyr-  
7 role (PY) was performed for preparing conductive hydrogels. By  
8 tuning the reaction conditions, the conductive components can  
9 permeate spontaneously and exclusively into the hydrogels to  
10 achieve required conductivity.<sup>[5,38–40]</sup>

11 Moreover the dye used for obtaining the 3D printed struc-  
12 tures was employed as dopant for PPY, enhancing the elec-  
13 trical conductivity.<sup>[6,41,42]</sup> If compared with other methods  
14 proposed in the literature,<sup>[12,13,43]</sup> this two-step approach can  
15 provide a higher control over the structure of the conductive  
16 hydrogel thanks to the formation of the conductive phase in a  
17 dedicated step that allows maintaining the defined 3D micro-  
18 architecture of the printed hydrogel, bringing to very precise  
19 and complex structures with electrical features. This approach  
20 has the potential to be extended to a wide variety of photo-  
21 sensitive hydrogels. The proposed strategy, coupling hydro-  
22 gels, 3D printing, and conductive polymers, could open new  
23 paths for the development of new bioelectrical interfaces for  
24 several biomedical applications, like complex systems for drug  
25 delivery or scaffolds for regenerative medicine but also in bio-  
26 energy fields or sensors.

## 29 2. Experimental Section

### 31 2.1. Materials

32 Poly(ethylene glycol)diacrylate (PEGDA) with a molec-  
33 ular weight of 700 g mol<sup>-1</sup> and PY reagent grade 98%  
34 were purchased from Sigma-Aldrich and used as received.  
35 Phenylbis(2,4,6-trimethylbenzoyl)phosphine oxide, selected as  
36 photoinitiator (PI) for its fair absorbing characteristics in the  
37 deep blue to near UV, and the dye, methyl orange (MO), were  
38 purchased from Sigma-Aldrich and used as received. Iron(III)  
39 chloride hexahydrate (FeCl<sub>3</sub> · 6H<sub>2</sub>O) was purchased from Alfa  
40 Aesar.

### 44 2.2. Fabrication of 3D PPY/PEGDA Structure

45 3D printable mixtures containing PEGDA, MO 0.2 phr (per  
46 hundred resin), and distilled water (dH<sub>2</sub>O) in different concen-  
47 tration (40, 50, 60, and 70% w/w) were prepared. 2 phr PI with  
48 respect to the PEGDA amount was added in the formulation.  
49 The 3D printing was performed on a PICOplus39, Asiga, with  
50 an X-Y resolution of 39 μm and light intensity of 30 mW cm<sup>-2</sup>.  
51 The digital models of structures were designed and converted  
52 to sterolithography (STL) file format for 3D printing. The layer  
53 thickness was set to 25 μm and the exposure time varied from 2  
54 to 15 s for increasing amounts of water.

55 Pyrrole monomers were dissolved in cyclohexane (0.5 M PY)  
56 while ferric chloride was dissolved in deionized water (0.3 M  
57 FeCl<sub>3</sub>). First the 3D parts were soaked for 1 h in the aqueous  
58 solution containing ferric chloride. The hydrogel was then

carefully blotted and subsequently soaked in the organic solu-  
1 tion containing the pyrrole monomers. The monomer pyrrole  
2 and the oxidant FeCl<sub>3</sub> diffuse at the aqueous/organic interface,  
3 the polymerization occurs, and the PPY/PEGDA composite  
4 hydrogel is formed. The same procedure was conducted on the  
5 thin film for electrical measurement.

### 9 2.3. Characterization Methods

10 Real-time rheological measurements were performed using an  
11 Anton Paar rheometer (Physica MCR 302) in parallel plate mode  
12 with a Hamamatsu LC8 lamp with a visible bulb and a cutoff  
13 filter below 400 nm (light intensity was set to 30 mW cm<sup>-2</sup>).  
14 The UV curing set up is equipped with a lower plate in quartz  
15 that allows the irradiation of the sample during the measure-  
16 ment. The gap between the two plates was set to 0.1 mm and  
17 the sample was kept at a constant temperature (25 °C) and  
18 under constant shear frequency of 10Hz, light was turned  
19 on after 120 s in order to stabilize the system. Concomitant  
20 changes in viscoelastic material moduli during polymerization  
21 were measured as a function of exposure time. The experiment  
22 was performed in the linear viscoelastic region with a strain  
23 amplitude of 0.5%. The morphological characterization of the  
24 3D printed materials after the interfacial polymerization of PY  
25 was carried out by scanning electron microscopy (SEM, Hitachi  
26 TM3030Plus). ATR spectra were collected on a Tensor 27 FTIR  
27 spectrometer (Bruker). The averaged signal was collected with  
28 a resolution of 2 cm<sup>-1</sup> from 4000 to 400 cm<sup>-1</sup>. X-ray photoelec-  
29 tron spectroscopy (XPS) was carried out by using a PHI 5000  
30 VersaProbe (Physical Electronics) system. The X-ray source was  
31 a monochromatic Al Kα radiation. Depth profile, by means of  
32 an Ar+ flux at 2 kV accelerating voltage, was performed on the  
33 sample in an alternate mode with sputtering cycles of 1 min  
34 each. Spectra were analyzed using Multipak 9.7 software.  
35 All core-level peak energies were referenced to C1s peak at  
36 284.5 eV (C–C/C–H) and the background contribution in HR  
37 scans was subtracted by means of a Shirley function. Differen-  
38 tial scanning calorimetry (DSC) measurements were performed  
39 with a Netzsch DSC 204 F1 Phoenix instrument, equipped with  
40 a low-temperature probe, between –80 and 60 °C with a heating  
41 rate of 10 °C min<sup>-1</sup> in nitrogen atmosphere. For each sample,  
42 the same heating module was applied two times and the final  
43 heat flow value recorded during the second heating cycle. The  
44 T<sub>g</sub> was defined as the midpoint of the heat capacity change  
45 observed in the DSC thermogram. Thermogravimetric analysis  
46 (TGA) was performed using a Netzsch TG 209 F1 Libra instru-  
47 ment in the range between 25 and 700 °C, with a heating rate  
48 of 10 °C min<sup>-1</sup> in nitrogen. Prior to the measurement all the  
49 samples were dried overnight in a vacuum oven in order to  
50 avoid the drop of weight relative to the water/moisture eventu-  
51 ally present in the sample. Compression tests were carried out  
52 using a dynamometer (Deben Microtest) equipped with a load  
53 cell of 200N. Alveolar structures were tested, and at least three  
54 specimens for each sample were tested. Samples resistivity  
55 was measured by using a Keithley-238 High Current Source  
56 Measure Unit (voltage range ±10 V, step 0.1 V), realizing a two-  
57 point contact setup placing copper electrodes on the two oppo-  
58 site basal sides. The data showed were obtained by multiple  
59

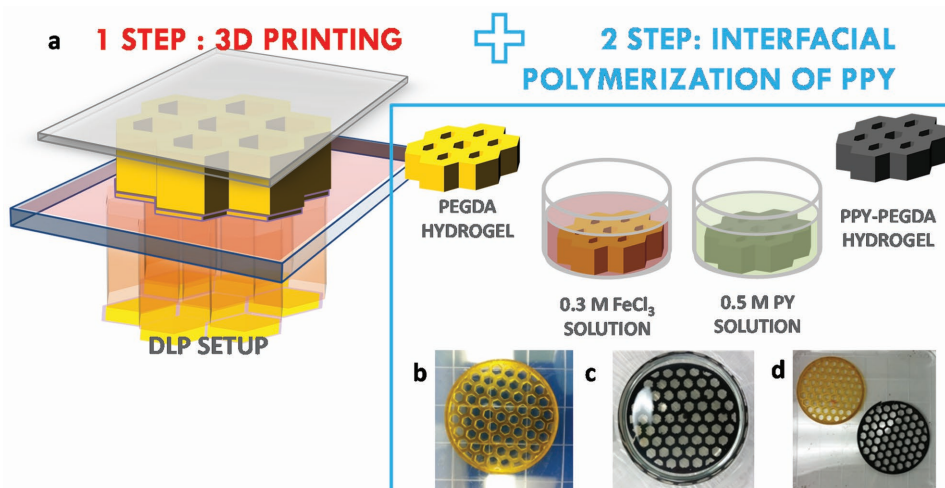


**Figure 1.** a) Sketch of the process. b) 3D printed PEGDA structure. c) PEGDA structure in PY/CYH solution. d) 3D PEGDA and 3D PEGDA/PPY structures.

measurements on different samples (three for each formulation). The electrical measurements on 3D printed structures were carried out with an apparatus composed of a Keithley 2750 multimeter and realizing a two-point contact setup, placing one copper electrode on each side of the structure.

### 3. Results and Discussion

In this work hybrid PPY/PEGDA conductive hydrogels were created through a two-step procedure. First a DLP 3D printing system was used to fabricate PEGDA microstructures and then PY was oxidized to PPY, exploiting an interfacial polymerization mechanism. Following this route, PPY could be formed into the PEGDA matrix, thus creating a conductive 3D printed hydrogel (Figure 1a).

The developed process is sketched in Figure 1a. 3D PEGDA hydrogel was printed by a DLP machine and then the 3D printed parts were soaked for 1 h in an aqueous solution containing ferric chloride: thanks to the high swell ability of PEGDA networks, the oxidant agent was incorporated in the 3D printed structure. The hydrogels were then carefully blotted and subsequently soaked again in an organic solution

containing pyrrole monomers. The polymerization to PPY involves the oxidation of the pyrrole monomer with ferric ions, the pyrrole monomers and the initiator diffuse at the aqueous/organic interface, and thus the polymerization is triggered. The reaction of PY with aqueous ferric chloride ( $\text{FeCl}_3$ ) is rapid and the PPY product is in the form of a black powder. After 1 h, the 3D parts are removed from the solution and immersed in  $\text{dH}_2\text{O}$  for at least 1 d to leach out low molecular weight components.

Different hydrogel formulations were prepared; MO was used both as dopant for the PPY<sup>[44,45]</sup> and as dye to improve the 3D printing resolution.<sup>[22–24]</sup>  $\text{dH}_2\text{O}$  was added in different amounts (40, 60, and 70% w/w) in the formulations in order to adjust the concentration (Figure 2a); the higher is the amount of initial water present in the formulation and, thus in the printed part, the higher will be the hydrogel ability of swelling in the subsequent steps (oxidant solution) and therefore the interfacial polymerization will be probably more efficient. Before printing the formulations, their reactivity was investigated by means of photorheology aiming to check the influence of the high amount of water added to the monomers on the light-induced crosslinking reaction. As expected, the higher the amount of water, the slowest the curing process as shown by the time-dependent elastic modulus ( $G'$ ) values reported in

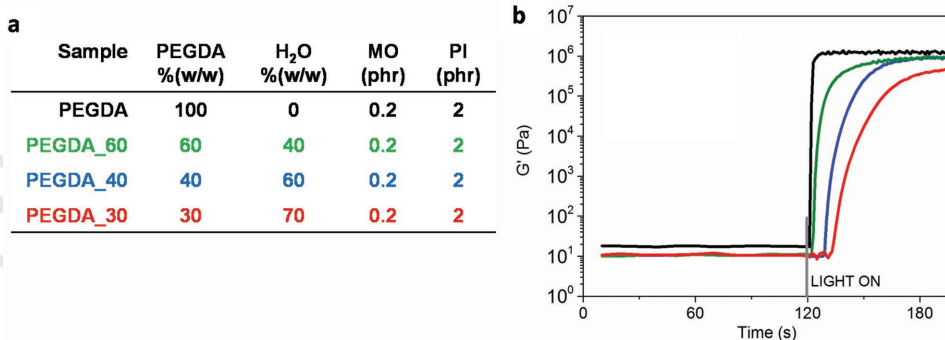


**Figure 2.** a) 3D printed formulations composition. b) Photorheology characterization of the different formulations.

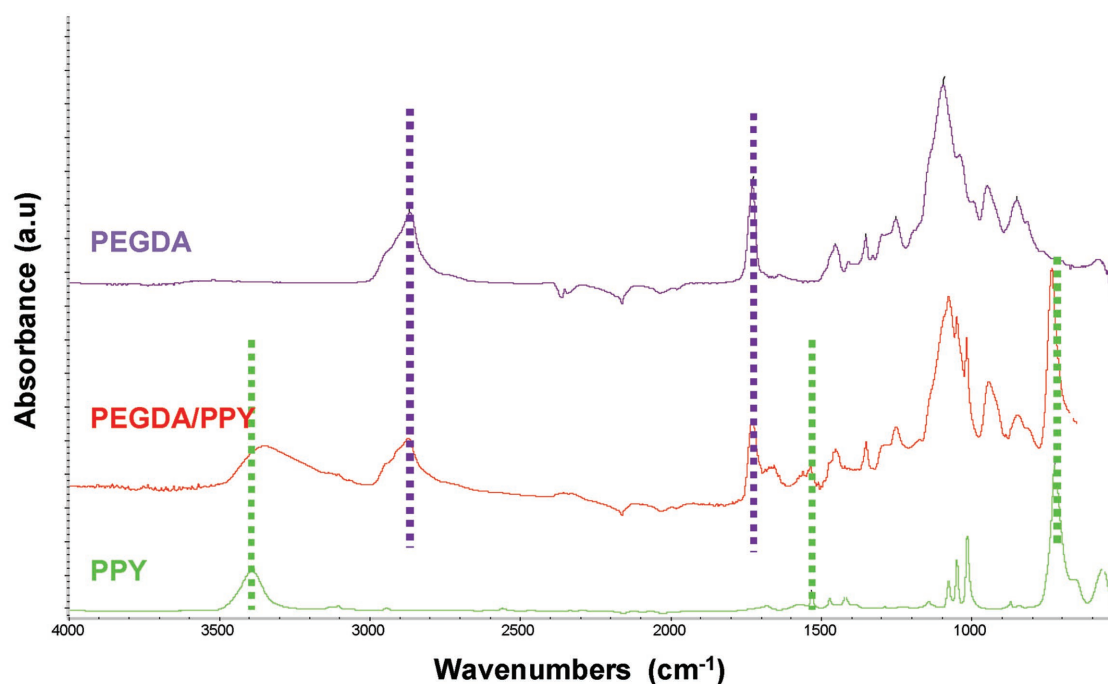


**Figure 3.** ATR spectra of pure PY (green), PPy/PEGDA hydrogel (red), and PEGDA hydrogel (purple).

Figure 2b. While the  $G$  curve relative to neat PEGDA starts increasing almost instantaneously after turning on the light and reaches its postcuring plateau in few seconds, the other formulations show a delay in the beginning of the reaction and a slower kinetic revealed by the lower slope of the curves. This effect results in the need of a longer exposition time during the printing process when the formulations containing higher amounts of water are printed. The use of higher amounts of water also induces a slight reduction of the  $G$  modulus after curing; in all the cases the obtained values are in line with those reported for other crosslinked hydrogels measured in similar conditions (amplitude and frequency).<sup>[46]</sup>

ATR spectroscopy was used to characterize the interfacial polymerization; the spectra are shown in Figure 3. The spectrum of neat PPY illustrates absorption peaks at 3402, 1528, 1418, and 1046  $\text{cm}^{-1}$  that could be assigned to the N–H, C–C, C–N stretching vibrations, and C–H in-plane vibrational bands of the pyrrole ring, respectively, and the peak at 1309  $\text{cm}^{-1}$  is assigned to C–N bonds.<sup>[7]</sup> In the PEGDA spectrum, the strong peak at 1724  $\text{cm}^{-1}$  could be assigned to the C=O stretching from ester bonds, while the broad band centered at 2862  $\text{cm}^{-1}$  can be assigned to the C–H (–CH, –CH<sub>2</sub>, and CH<sub>3</sub>) stretching vibration. In the FTIR of the PEGDA/PPY hydrogel, it is possible to identify characteristic peaks of both polypyrrole, at 3396, 1528, 1465  $\text{cm}^{-1}$ , and PEGDA, peak at 1724 and 2862  $\text{cm}^{-1}$ , indicating the presence of both polymers blended. This confirms the successful formation of PPY on PEGDA matrix (Figure 3).

Detailed images of 3D printed structures with optical microscopy and SEM are shown in Figure 4. Well-defined architecture and good building accuracy of complex objects were achieved; details down to 200  $\mu\text{m}$  were achieved. This value represents the experimental limit observed for this kind of water-based

formulations. Moreover, the PPY postpolymerization process on the printed structures does not worsen the resolution achieved during the printing step: the structures in fact remain intact without cracks. The surface after the polymerization of PPY was evaluated by SEM. While the surface of PEGDA structures is smooth, a certain roughness was evident after PPY polymerization, with a flowerlike pattern and big porosity (Figure 4c). Probably this could be related to the high concentration of PY monomers in the solution, which leads to a faster polymerization rate and thus a more uneven distribution of PPY.<sup>[47]</sup> Thicker samples (4 mm) were also produced and their cross section was observed by SEM analyses in order to evaluate the PPY distribution into the sample. As visible in Figure 4d,e, PPY forms spherical island in all the thickness of the sample showing a complete interpenetration of the two polymers.

TGA analyses were performed in order to determine the influence of PPY created in the interfacial polymerization step on thermal stability of the object and characterize the amount of PPY deposited (Figure 5). The acidic dopants of the PPY are volatilized upon heating,<sup>[48]</sup> which explains why the PEGDA/PPY hydrogels show lower thermal stability than that of PEGDA ones below 350 °C. As expected, PEGDA/PPY hydrogel left more residue at 700 °C in comparison to the sample without PPY (Figure 5). Moreover this residue increases as the increasing of water in the initial formulation. This could be related to the fact that the more the structure is swellable, the more free space is available for PPY infiltration. This relationship between cross-linking density and the amount of water in the initial formulation could also be observed in the decrease of  $T_g$  measured by DSC. In fact, the more the hydrogel is swelled during its formation (which means the higher its water content), the lower is the cross-linking density.<sup>[49]</sup> DSC measurements were also performed on treated PEGDA/PPY samples.

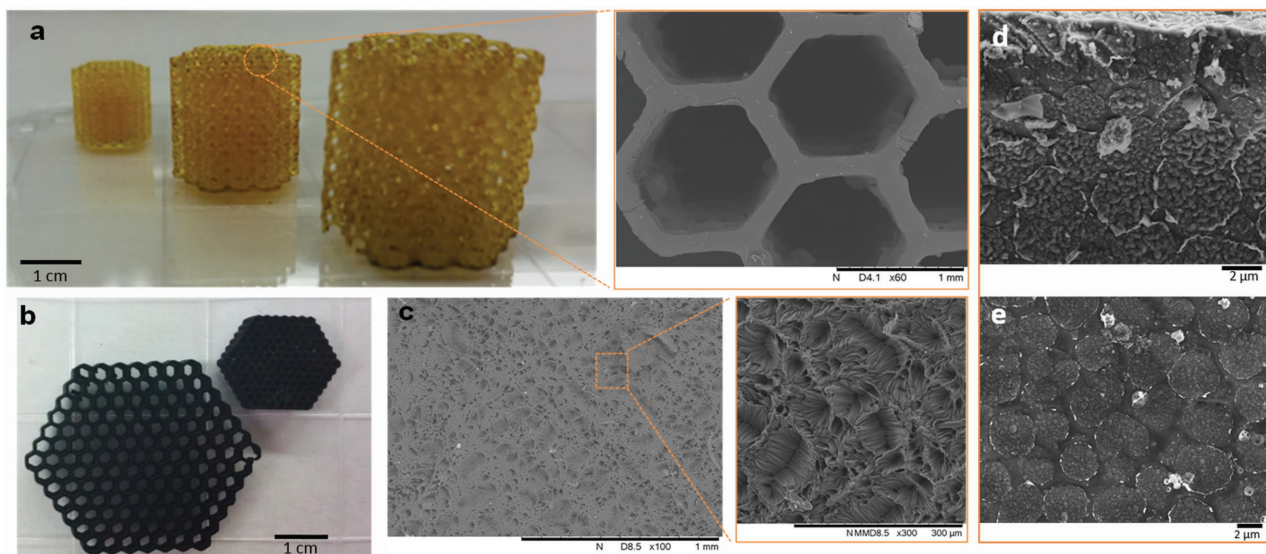
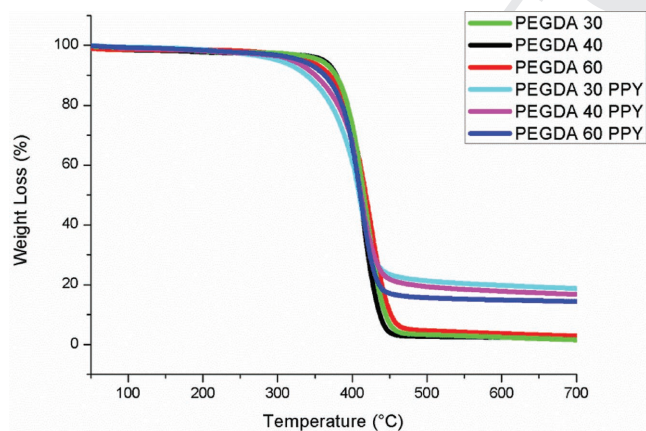


**Figure 4.** a) Example of a honeycomb structure printed in different dimension (PEGDA\_40) and SEM detail of the features obtained. b) 3D printed PEGDA-PPY honeycomb structures. c) SEM images of the pyrrole surface. d,e) Cross section of a thick sample (4 mm).

The presence of a second polymeric phase hinders PEGDA chain mobility resulting in the increase of  $T_g$ .

XPS measurements have been performed on sample PEGDA 30\_PPY surface in order to obtain information regarding the chemical composition of its first layers ( $\leq 10$  nm). In **Figure 6a** we report the survey spectrum of the sample: we detected C (59.4 at%), O (26.0 at%), N (5.7 at%), and some impurities due to Cl (0.5 at%) and Si (8.5 at%). We then performed high resolution analysis on the C1s peak (as reported in **Figure 6b**).



Sample	$T_5$ (°C)	Residue	$T_g$ (°C)*
PEGDA_60	355	2.3	-42
PEGDA_40	360	1.5	-48
PEGDA_30	357	2.8	-50
PEGDA_60_PPY	330	14.4	-30
PEGDA_40_PPY	319	16.7	-39
PEGDA_30_PPY	301	18.7	-45

\*DSC value

**Figure 5.** TGA plots and thermal properties of the compositions. \* $T_5$  represents the temperature at which the 5% in weight is lost.

We attributed four components to the raw signal in order to fit properly the experimental curve. The first component at 284.5 eV has been attributed to C–C/H or  $\alpha$ -carbons bonds,<sup>[50]</sup> the second at 286.1 eV to  $\alpha$ -carbons, the third one at 287.4 eV to  $\alpha$ -carbons adjacent to positively charged N atoms ( $C\alpha^*$ ), and the last one at 288.3 eV at carbon atoms bonded with oxygen species (–C=O or –COO–).<sup>[51]</sup> The same procedure has also been applied to the N1s peak (**Figure 6c**), obtaining four components: imine –N = (398.2 eV), amine –NH– (399.4 eV), protonated amine –NH<sub>2</sub><sup>+</sup> (400.1 eV), and protonated imine = NH– (401.5 eV).<sup>[52]</sup>

A further analysis has been accomplished to observe the homogeneity of PPY inclusion in the PEGDA matrix, at least in the first layers. To obtain this information we performed a depth profile measurements, using Ar<sup>+</sup> as sputtering source. We alternated sputtering cycle (1 min) with HR measurements in the N1s region. We repeated the procedure for 60 cycles (60 min) obtaining the profile reported in **Figure 6d**. As can be clearly seen, the intensity of the nitrogen signal is almost constant during all the measurement. A rough estimation of the polymeric composite depth sputtered can be done according to the literature,<sup>[53]</sup> by considering a sputter rate of the order of 10 nm min<sup>-1</sup> and then obtaining a 600 nm depth. Along this sputtering depth PPY distribution as expected from SEM observations.

Electrical measurements were performed on films in order to evaluate the influence of PPY on the resistivity. As reported in **Figure 7** the presence of PPY decreases the films' resistivity of one order of magnitude or more. This indicates that a continuous PPY network was successfully formed with interfacial polymerization. The resistivity values obtained are in good agreement with values reported in the literature of similar systems.<sup>[54]</sup> It is also important to underline that all the new formulations showed a resistivity considerably lower than PEGDA photocured without water.<sup>[15]</sup> Moreover, the more the water in the initial formulation, the lower the resistivity measured. In

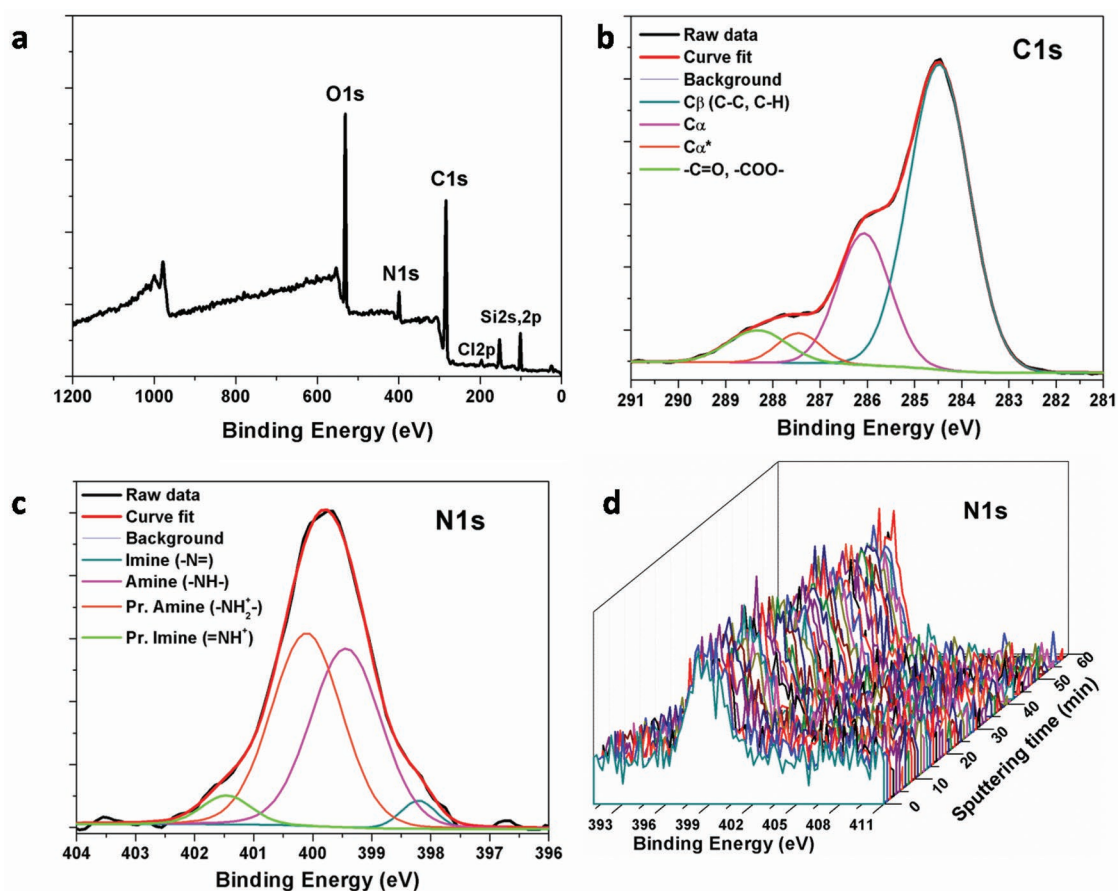


**Figure 6.** a) Sample PEGDA\_30\_PPY XPS survey spectrum; b,c) XPS high-resolution core level peaks for C1s and N1s along with their deconvolution procedure results; d) XPS depth profile curves for N1s peak (Ar+ source at 2 kV, alternate sputtering with 1 min cycle each).

order to clarify this point, electrical measurements were performed on the same neat PEGDA samples after drying in a vacuum oven overnight. All the samples showed higher resistivity (2 MΩcm), which is consistent with the literature. This let us believe that some water/humidity could remain trapped in the polymeric network during material synthesis, thus reducing resistivity. However, this assumption seems to us not sufficient

to explain the low resistivity values measured for PEGDA\_30 sample and more investigations are ongoing to deepen this point. The same vacuum treatment was performed on the samples with PPY, which did not show significant change in the electrical behavior.

In order to evaluate the mechanical properties of the samples, honeycomb structures were printed and tested in compression

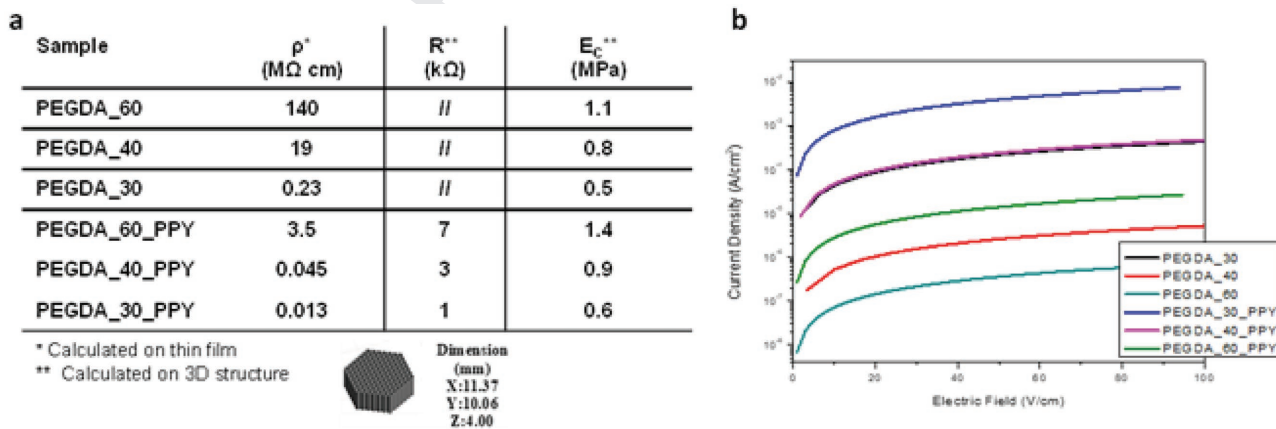


**Figure 7.** a) Table reporting electrical resistivity and electrical resistance and Young's modulus; b) semilogarithmic plot of I/V measurements and resistance evaluation for the different samples.

1 tests. The table in Figure 7a reports the Young's modulus for  
2 each formulation under compression. The measurements per-  
3 formed on the structures showed that the Young's modulus is  
4 higher in the presence of PPY compared to PEGDA sample  
5 without PPY, which can explain that the presence of a second  
6 phase hinders the PEGDA chain mobility as already seen in the  
7 DSC. Finally, the resistance of 3D printed conductive hydrogel  
8 structures was also measured, confirming the trend observed  
9 on films.

#### 4. Conclusions

14 In this paper, we reported a novel approach for the fabrica-  
15 tion of electrically conductive, mechanically tough 3D printed  
16 hydrogels by coupling interfacial polymerization of PPY with  
17 3D printing technology. It was demonstrated that precise 3D  
18 structures of PEG-based hydrogels can be realized even with a  
19 considerable high amount of water in the initial formulation.  
20 The honeycomb structures were successfully infiltrated with  
21 PPY by interfacial polymerization; ATR, XPS, and SEM results  
22 indicate the existence of PPY within the matrix. Moreover the  
23 dye used for enhancing 3D printing precision was exploited for  
24 PPY doping. The developed structures were electrically conduc-  
25 tive and mechanically tough. This strategy could be applied for  
26 developing a new bioelectronics interface for several biomedical  
27 applications.

#### Acknowledgements

32 The authors are grateful for the financial support from the Natural  
33 Science and Engineering Research Council of Canada (NSERC), the  
34 Canada Foundation for Innovation (CFI), and the University of Western  
35 Ontario.

#### Conflict of Interest

39 The authors declare no conflict of interest.

#### Keywords

44 3D printing, interfacial polymerization, PEGDA, photopolymerization

Received: July 22, 2017  
Revised: November 1, 2017  
Published online:

- 52 [1] G. Justin, A. Guiseppi-Elie, *Biomacromolecules* **2009**, *10*, 2539.  
53 [2] C. J. Small, C. O. Too, G. G. Wallace, *Polym. Gels Networks* **1997**, *5*,  
54 251.  
55 [3] Y.-x. Zhao, K.-f. Ren, Y.-x. Sun, Z.-j. Li, J. Ji, *RSC Adv.* **2014**, *4*, 24511.  
56 [4] A. Guiseppi-Elie, *Biomaterials* **2010**, *31*, 2701.  
57 [5] Y. Xiao, L. He, J. Che, *J. Mater. Chem.* **2012**, *22*, 8076.  
58 [6] J. Ji, et al., *J. Macromol. Sci., Part B: Phys.* **2015**, *54*, 1122.  
59 [7] H. P. de Oliveira, S. A. Sydlik, T. M. Swager, *J. Phys. Chem. C* **2013**,  
117, 10270.

- [8] Y. Wu, et al., *J. Mater. Chem. B* **2015**, *3*, 5352.  
[9] S. Naficy, J. M. Razal, G. M. Spinks, G. G. Wallace, P. G. Whitten,  
*Chem. Mater.* **2012**, *24*, 3425.  
[10] H. Huang, J. Wu, X. Lin, L. Li, S. Shang, M. C. Yuen, G. Yan, *Carbo-  
hydr. Polym.* **2013**, *95*, 72.  
[11] C. Vallejo-Giraldo, A. Kelly, M. J. P. Biggs, *Drug Discovery Today*  
**2014**, *19*, 88.  
[12] Y. Zhao, B. Liu, L. Pan, G. Yu, *Energy Environ. Sci.* **2013**, *6*, 2856.  
[13] J. Stejskal, *Chem. Papers*, *1*.  
[14] Y. L. Kong, I. A. Tamargo, H. Kim, B. N. Johnson, M. K. Gupta,  
T.-W. Koh, H.-A. Chin, D. A. Steingart, B. P. Rand, M. C. McAlpine,  
*Nano Lett.* **2014**, *14*, 7017.  
[15] J. N. Hanson Shepherd, S. T. Parker, R. F. Shepherd, M. U. Gillette,  
J. A. Lewis, R. G. Nuzzo, *Adv. Funct. Mater.* **2011**, *21*, 47.  
[16] R. Suntornnond, J. An, C. K. Chua, *Macromol. Mater. Eng.* **2017**,  
*302*, 1600266.  
[17] M. Zhou, B. H. Lee, L. P. Tan, *Int. J. Bioprint.* **2017**, *3*, 2017.  
[18] J. C. McDonald, M. L. Chabiny, S. J. Metallo, J. R. Anderson,  
A. D. Stroock, G. M. Whitesides, *Anal. Chem.* **2002**, *74*, 1537.  
[19] B. C. Gross, J. L. Erkal, S. Y. Lockwood, C. Chen, D. M. Spence,  
*Anal. Chem.* **2014**, *86*, 3240.  
[20] J. Z. Manapat, Q. Chen, P. Ye, R. C. Advincula, *Macromol. Mater.  
Eng.* **2017**, *302*, 1600553.  
[21] X. Wang, Q. Guo, X. Cai, S. Zhou, B. Kobe, J. Yang, *ACS Appl. Mater.  
Interfaces* **2014**, *6*, 2583.  
[22] E. Fantino, A. Chiappone, F. Calignano, M. Fontana, F. Pirri,  
I. Roppolo, *Materials* **2016**, *9*, 589.  
[23] A. Chiappone, E. Fantino, I. Roppolo, M. Lorusso, D. Manfredi,  
P. Fino, C. F. Pirri, F. Calignano, *ACS Appl. Mater. Interfaces* **2016**,  
*8*, 5627.  
[24] E. Fantino, A. Chiappone, I. Roppolo, D. Manfredi, R. Bongiovanni,  
C. F. Pirri, F. Calignano, *Adv. Mater.* **2016**, *28*, 3712.  
[25] S. Stassi, E. Fantino, R. Calmo, A. Chiappone, M. Gillono,  
D. Scaiola, C. F. Pirri, C. Ricciardi, A. Chiadò, I. Roppolo, *ACS Appl.  
Mater. Interfaces* **2017**, *9*, 19193.  
[26] J. Malda, J. Visser, F. P. Melchels, T. Jüngst, W. E. Hennink,  
W. J. Dhert, J. Groll, D. W. Huttmacher, *Adv. Mater.* **2013**,  
*25*, 5011.  
[27] J.-Y. Sun, X. Zhao, W. R. Illeperuma, O. Chaudhuri, K. H. Oh,  
D. J. Mooney, J. J. Vlassak, Z. Suo, *Nature* **2012**, *489*, 133.  
[28] N. B. Graham, in *Poly(Ethylene Glycol) Chemistry: Biotechnical and  
Biomedical Applications* (Ed: J. M. Harris), Springer, Boston, MA  
**1992**, pp. 263–281.  
[29] J. M. Harris, *Poly (Ethylene Glycol) Chemistry: Biotechnical and Bio-  
medical Applications*, Springer Science & Business Media, Berlin,  
Germany **2013**.  
[30] K. Arcaute, L. Ochoa, F. Medina, C. Elkins, B. Mann, R. Wicker,  
*MRS Online Proceedings Library* **2005**, *874*.  
[31] V. Chan, J. H. Jeong, P. Bajaj, M. Collens, T. Saif, H. Kong, R. Bashir,  
*Lab Chip* **2012**, *12*, 88.  
[32] V. Chan, P. Zorlutuna, J. H. Jeong, H. Kong, R. Bashir, *Lab Chip*  
**2010**, *10*, 2062.  
[33] A. Chiappone, I. Roppolo, E. Naretto, E. Fantino, F. Calignano,  
M. Sangermano, F. Pirri, *Composites, Part B: Eng.* **2017**, *124*, 9.  
[34] X. Wang, M. Jiang, Z. Zhou, J. Gou, D. Hui, *Composites, Part B: Eng.*  
**2017**, *110*, 442.  
[35] N. Nuraje, K. Su, *ACS Nano* **2008**, *2*, 502.  
[36] G. Qi, Z. Wu, H. Wang, *J. Mater. Chem. C* **2013**, *1*, 7102.  
[37] J. Bhadra, D. Sarkar, *Indian J. Phys.* **2010**, *84*, 1321.  
[38] D. Zhang, F. Di, Y. Zhu, Y. Xiao, J. Che, *J. Bioact. Compat. Polym.:  
Biomed. Appl.* **2015**, *30*, 600.  
[39] N. V. Blinova, M. Trchová, J. Stejskal, *Eur. Polym. J.* **2009**,  
*45*, 668.  
[40] M. Karbarz, M. Gniadek, M. Donten, Z. Stojek, *Electrochem.  
Commun.* **2011**, *13*, 714.



1	[41] X. Tuo, B. R. Li, C. L. Chen, Z. L. Huang, H. B. Huang, L. Li, <i>Synth. Met.</i> <b>2016</b> , 213, 73.	[48] Y. Liao, T. P. Farrell, G. R. Guillen, M. Li, J. A. T. Temple, X.-G. Li, E. M. V. Hoek, R. B. Kaner, <i>Mater. Horiz.</i> <b>2014</b> , 1, 58.	1
2	[42] S. Ying, W. Zheng, B. Li, X. She, H. Huang, L. Li, Z. Huang, Y. Huang, Z. Liu, X. Yu, <i>Synth. Met.</i> <b>2016</b> , 218, 50.	[49] L. M. Weber, C. G. Lopez, K. S. Anseth, <i>J. Biomed. Mater. Res., Part A</i> <b>2009</b> , 90, 720.	2
3	[43] N. Saengchairat, T. Tran, C.-K. Chua, <i>Virtual Phys. Prototyping</i> <b>2017</b> , 12, 31.	[50] P. M. Carrasco, M. Cortazar, E. Ochoteco, E. Calahorra, J. A. Pomposo, <i>Surf. Interface Anal.</i> <b>2007</b> , 39, 26.	3
4	[44] J. Feng, W. Yan, L. Zhang, <i>Microchim. Acta</i> <b>2009</b> , 166, 261.	[51] N. Garino, A. Sacco, M. Castellino, J. A. Muñoz-Tabares, A. Chiodoni, V. Agostino, V. Margaria, M. Gerosa, G. Massaglia, M. Quaglio, <i>ACS Appl. Mater. Interfaces</i> <b>2016</b> , 8, 4633.	4
5	[45] X. Yang, Z. Zhu, T. Dai, Y. Lu, <i>Macromol. Rapid Commun.</i> <b>2005</b> , 26, 1736.	[52] S. Golczak, A. Kancierzewska, M. Fahlman, K. Langer, J. J. Langer, <i>Solid State Ionics</i> <b>2008</b> , 179, 2234.	5
6	[46] H. Tai, W. Wang, T. Vermonden, F. Heath, W. E. Hennink, C. Alexander, K. M. Shakesheff, S. M. Howdle, <i>Biomacromolecules</i> <b>2009</b> , 10, 822.	[53] T. Nobuta, T. Ogawa, <i>J. Mater. Sci.</i> <b>2009</b> , 44, 1800.	6
7	[47] A. A. Jatrakar, J. B. Yadav, R. Deshmukh, H. C. Barshilia, V. Puri, <i>J. Phys. Chem. Solids</i> <b>2015</b> , 80, 78.	[54] G. Kaur, R. Adhikari, P. Cass, M. Bown, P. Gunatillake, <i>RSC Adv.</i> <b>2015</b> , 5, 37553.	7
8			8
9			9
10			10
11			11
12			12
13			13
14			14
15			15
16			16
17			17
18			18
19			19
20			20
21			21
22			22
23			23
24			24
25			25
26			26
27			27
28			28
29			29
30			30
31			31
32			32
33			33
34			34
35			35
36			36
37			37
38			38
39			39
40			40
41			41
42			42
43			43
44			44
45			45
46			46
47			47
48			48
49			49
50			50
51			51
52			52
53			53
54			54
55			55
56			56
57			57
58			58
59			59

## Query

- Q1: Please provide TOC keyword.
- Q2: Please provide the highest academic title (either Dr. or Prof.) for all authors, where applicable.
- Q3: Please define 'ATR and FTIR' at the first occurrence in the text.
- Q4: Please define 'HR' at the first occurrence in the text.
- Q5: Please confirm if the deletion of panel (a) from the caption of Figure 3 is correct.
- Q6: Please check that the edits to the sentence 'The same procedure has also been applied ...' are OK and that the meaning has not been changed.
- Q7: Please complete the sentence 'Along this sputtering depth PPY distribution as expected from SEM observations'.
- Q8: Please check that the edits to the sentence 'However, this assumption seems to us not sufficient ...' are OK and that the meaning has not been changed.
- Q9: Please check that the edits to the sentence 'The measurements performed on the structures ...' are OK and that the meaning has not been changed.
- Q10: Please check that the edits to the sentence 'The honeycomb structures were successfully ...' are OK and that the meaning has not been changed.
- Q11: The term 'et al.' is not permitted in the reference list. Please provide all author names in references (6).
- Q12: Please confirm if the authors in refs. (10, 14, 15, 18, 21–27, 31, 33, 41, 42, 46–48, and 51) are correct as included.
- Q13: Please provide year of publishing and volume number in ref. (13).
- Q14: Please confirm if the year and volume number in ref. (20) are correct as included.
- Q15: Please confirm if the publisher name is correct as edited in ref. (28).
- Q16: Please confirm if the publisher location in ref. (29) is correct as included.
- Q17: Please provide page number in ref. (30), if available.

